Analysis of blink dynamics in patients with blepharoptosis

Felix H.W. Mak[1], Anthony Harker[3], Kyung-Ah Kwon[1,†], Mohan Edirisinghe[1*], Geoffrey E. Rose[2], Fabiola Murta[2], Daniel G. Ezra[2]

[1]Department of Mechanical Engineering, University College London, Torrington Place, London, WC1E 7JE, UK

[2]Moorfields Eye Hospital, UCL Institute of Ophthalmology NIHR Biomedical Research Centre for Ophthalmology, 162 City Road, London, EC1V 2PD, UK

[3]Department of Physics & Astronomy, Faculty of Mathematics & Physical Sciences, University College London, Gower Street, London, WC1E 6BT, UK

† Present address: Department of Materials Science and Metallurgy, University of Cambridge, 27 Charles Babbage Road, Cambridge, CB3 0FS, UK

*Corresponding author: m.edirisinghe@ucl.ac.uk

Abstract

Due to the rapid movements of the human upper eyelid, a high speed camera was used to record and characterise voluntary blinking and the blink dynamics of blepharoptosis patients were compared to a control group.

Twenty-six blepharoptosis patients prior to surgery and 45 control subjects were studied and the vertical height of the palpebral aperture was measured manually at 2ms intervals during each blink cycle. The palpebral aperture and blinking speed were plotted with respect to time and a predictive model was generated. The blink dynamic was analysed in closing and opening phases, and revealed a reduced speed of the initial opening phase in

ptotic patients, suggesting intrinsic muscle function change in ptosis pathogenesis. The palpebral aperture versus time curve for each subject was reconstructed using custom-built parameters, however there were significant differences between the two groups. Those parameters used included the rate of closure, the delay between opening and closing, rate of initial opening, rate of slow opening (non-linear function) and the "switch point" between those two rates of opening. The model was tested against a new group of subjects and was able to discriminate ptosis patients from controls with 80% accuracy.

1. Introduction

Blepharoptosis, also known as "ptosis", is characterised by abnormal drooping of the upper eyelid and affected individuals have difficulty raising their lids to the normal vertical palpebral aperture of about 9-12mm (1). Although there is ethnic variation in the palpebral aperture, in particular, it is significantly smaller in Asian ethnic groups (2), the severity of ptosis can be usefully measured by the palpebral aperture.

Ptosis, which can be congenital or acquired, can affect one (unilateral) or both eyes (bilateral), and may be due to many different factors. The acquired form is most commonly observed as an age-related involutional change characterised by levator aponeurosis dehiscence, referred to as "an aponeurotic ptosis" (3). However, it can arise from a wide range of causes which include: trauma; mechanical effects, eyelid masses; neurological defects, such as 3rd cranial nerve palsy, or Horner's syndrome; or myogenic causes in diseases such as myotonic dystrophy or mitochondrial myopathy. In severe ptosis the visual axis may be obscured by the eyelid causing functional blindness.

Myogenic and neurological causes of ptosis generally involve weakness of the levator palpebrae superioris (LPS) muscle that lifts the upper eyelid during opening. The precise mechanism for development of an aponeurotic ptosis is poorly understood, but has been suggested to arise from a disinsertion of the levator muscle from the tarsal plate (3-5) and would therefore, in theory, affect the blinking dynamics. At present, manual measurement of the palpebral aperture height and the eyelid excursion ("LPS muscle function") are the sole determinants for diagnosing ptosis. This method also involves experienced judgements at early stages of the disease. Our limited knowledge of blinking dynamics in ptotic patients suggested that an accurate and detailed analysis of the blink cycle could further our understanding of diseased blinking dynamics compared to normal eyes. In addition, appropriate modelling of the blink cycle may enable clinicians to diagnose ptosis more accurately and at an earlier stage, where the condition is less likely to be of concern to the patients. Subsequently, this can also provide avenues for monitoring and adequate treatment.

Characteristics of blink dynamics such as height of the palpebral aperture, blink speed, duration and frequency vary significantly between healthy and affected groups, but no data has been published to compare the blink dynamics of patients with ptosis as compared with unaffected subjects. Blink dynamics have been studied by placing electrodes immediately above the eyebrow and below the lower eyelid, and amplifying these oculometric signals for offline analysis (6). Static image analysis using a high-speed camera has also been used (7). Also, other techniques, such as infrared-oculography (8) or a magnetic search-coil technique have been used to investigate the rapid blink movements (9-12).

In this work, a high-speed camera was used to record the voluntary motion of eye blinking in patients suffering from ptosis. For each blink cycle in individual patients, the images were analysed for central height of the palpebral aperture as a function of time. A model was constructed to quantify the characteristics of ptotic blink dynamics, and the results compared with those for healthy subjects. Linear discriminant analysis (LDA) and Gaussian classification were used to discriminate between diseased and healthy subjects and the results could potentially improve clinical evaluation and provide a reliable method for the diagnosis and quantification of ptosis.

2. Experimental details

2.1 Subject selection

There is ethnic variability in facial structure, especially between Western and Oriental Asian faces, the dominant features of the Asian face being a significantly wider intercanthal distance and a narrower vertical palpebral aperture (PA) as well as a wider facial contour compared to Caucasian subjects (2). These differences in facial structures might be reflected in varied muscle attachments and, combined with a narrower PA, this might affect the blink mechanics and dynamics that were measured in this study. Consequently, volunteers of Oriental origin (very few in number) were excluded from the study. The study received local ethical approval.

Twenty-six ptosis patients (11 males, 15 females) and 45 healthy volunteers (14 males, 31 females), including the 25 healthy subjects from our previous study (13) were included in the present work. A comparative histogram of the probability distribution of values of the

discriminant function was plotted and confirmed that there is no statistically significant difference between the genders.

All ptosis patients were awaiting surgical correction of their aponeurotic disinsertion ptosis and were recruited from the oculoplastic service at Moorfields Eye Hospital NHS Foundation Trust. Ptosis patients ranged from age 22 to 84 (mean of 52) years, and the control range was 25 to 67 years (mean of 41) (detailed breakdown of the different ptosis conditions are supplied in supplementary information 1). Seven additional subjects (1 male, 6 females) were not used for primary mathematical modelling, but were used retrospectively to assess for reliability of the derived model.

Control data was collected using two different cameras, with frame-rates of 500fps and 600fps measurements taken every 5ms - to give an effective frame-rate of 200fps, as in our previous study (13). Subsequently, smooth curves were fitted to the raw data to ensure that differences in collection protocol had a negligible effect on the results.

2.2 Protocols

The present protocol followed the previously described principles introduced for analysis of blink dynamics using high-speed camera images (13), with only minor differences in the equipment used and analytical techniques. Ptosis patients who agreed to participate in this study had their blinking recorded by a high-speed camera and all participants were briefed before filming, explaining what would be measured and how it would be accomplished. After filming the patients had their ocular surface examined and key oculoplastic measurements were taken manually – namely, vertical PA; the maximum excursion of the upper eyelid margin in mm (“LF”); and “margin-reflex distance” (“MRD”), the distance between the central corneal light reflex and upper eyelid margin in primary gaze. LF is the

commonly employed standard for classifying LPS function, and the PA and MRD indicate the static severity of ptosis (1, 14, 15).

Subjects were seated comfortably in a controlled hospital environment at room temperature (22.6 ± 1.6°C) and standard humidity (28.3 ± 2.2%), with natural light (not directly shining on their faces). The high-speed camera was set-up at eye level in front of the subjects, and 12.3 seconds of high-speed recording of voluntary blinking was taken for each patient with a monochrome Photron Ultima APX12K Camera (Photron – Europe Limited, Buckinghamshire, UK), operating at 500fps with full 1024x1024 resolution; a total of 6144 frames per patient was recorded in 8bit grey scale. The camera was mounted with a Nikon f/2.8 macro zoom lens with focal length of 24-85mm. Subjects were asked to relax, look straight into the camera and blink as normally as possible; a brief pause prior to recording allowed the subjects to familiarise themselves and be as natural as possible. A verbal command was given before each blink was captured.

A desktop computer running Windows 7 operating system with the high speed camera's default software (Photron FASTCAM Viewer version 3.5.1.0) was used to capture the data, in real-time, and record it directly to an external hard-drive. All images were captured in RAW format and converted to TIFF, using the same software.

2.3 Method of analysis

Isolation of a complete blink (100% PA recovery) from each subject was attempted, it being considered a blink if their upper eyelid margin reached below 50% of the starting PA during the closure phase. Some subjects did not achieve 100% recovery, and were therefore analysed to the closest maximum percentage recovery. Only the affected eyes were considered in the ptosis patients and both eyes were included in the control group but were

not treated as pairs. The PA in 71 subjects was measured using open source freeware ("ImageJ" software; W. Rasband, National Institute of Mental Health, USA), the PA being determined by calibrating the horizontal corneal diameter to a standard of 11.70mm (16) and the central PA assessed in every frame of the recorded videos. The measurement started from the moment the upper eyelid descended and continued until the initial PA value was recovered, or until the eye ceased to open further. The resulting data was normalised to generate a comparable master curve (figures 1 & 2) in order to include patients with a range of PA measurements. Blink duration and peak blink speed were also analysed and compared to the control group. Blink frequency was not measured both because it is highly variable and also because this study focuses on voluntary blinking. Speeds were calculated as a magnitude from the upper lid excursion for each frame (that is, by a one-sided finite difference approximation). These results are presented in section 3.1. Means and standard errors of the means were calculated for both groups.

2.4 Statistical analysis

The measured RAW data were fed into a program written in Mathematica (Wolfram Research Champaign, Illinois, USA) and investigated using Fisher's linear discriminant analysis and Gaussian classifiers.

As ptosis is often age-dependent as discussed in section 3.3, this analysis has been carried out in several ways: i) Ptosis group *versus* control group (irrespective of age), data not shown. ii) Control subjects only – age 40 or over *versus* age below 40 (section 3.3). iii) Ptosis group *versus* control group – patients of age 40 or over only (section 3.4). The cut-off point for the control group at age 40 was chosen to select the best age-match for our two study

groups whilst maximising the sample size: for age ≥40, the mean control age became 51 years (with sample size of 22), compared to a mean age of 52 years for all 26 ptosis patients.

To model the eyelid motion in order to differentiate ptosis from controls, recreating the blinking profile was attempted. Key features of the PA *versus* time plot were separated into different parameters to fit a function to best represent these features (figure 3). These parameters include initial opening; time offset for closing; minimum opening; rapidity of closure; time offset for opening; rapidity of opening; time offset for slow opening; rapidity of slow opening and end point. Analysing the data was performed in order to allow Mathematica to characterise the ptotic blink dynamics and to determine if they are different from the control group. For this reason, another group of subjects was gathered from Moorfields Eye Hospital to act as masked controls in a retrospective test of our model. In this study, we have used the five parameters detailed in the next section (section 2.5).

2.5 Coding

There are two main aspects to the Mathematica coding: extracting parameters from the data and analysing them statistically. The time trace for each blink was first normalised, with the maximum PA set to 100%, and then divided into five segments, as follows (figure 3):

1. Constant at the initial PA, PA_{start}, from time 0 to t_1;
2. Constant-velocity closure at a rate v_1 to the minimum PA, PA_{min}, between t_1 and t_2;
3. Constant at PA_{min} from t_2 to t_3;
4. Constant-velocity opening at a rate v_2 from t_3 to the switching time (to the next parameter; change of rate of opening) t_4;
5. Smooth approach to full opening from t_4 to the end of the trace, $PA(t)=A+B \tanh(\alpha(t-t_4))$.

The values of A and B were determined by the value of PA at t_4 and by the requirement that the PA should asymptotically tend to its final value PA_{end} and the best fit of this piecewise smooth function was determined for each time trace by using Mathematica's *NonlinearModelFit* function. The fitted parameters were PA_{start} , PA_{end}. v_1, v_2, α, $t_{close}= (t_1+ t_2)/2$, t_{open} which is defined similarly to t_{close} as the time at which the PA would reach $(PA_{min}+PA_{end})/2$ at a rate v_2, and t_4, the switching time. The value of PA_{min} was not used as a fitting parameter, but was set to the observed minimum percentage PA.

The fitted parameters characterise the time trace, but in order to remove any constant offsets from the time traces the five quantities which were used for further analysis were v_1, v_2, α, $T_1= (t_{open}-t_{close})$ and $T_2= (t_4-t_{open})$. The measured value of PA_{min} was also taken into consideration, as it was observed that whilst healthy eyes were all able to close fully, some ptotic eyes could not: cases with full closure were analysed separately from those with partial closure.

The initial analysis was to assemble a linear combination of the five quantities described above which best distinguishes between ptotic and healthy eyelids, and this was done using the Fisher Linear Discriminant procedure (17), which maximises the ratio of "between-class" and "within-class" variances; this finds the best plane in the five-dimensional space of the parameters for separating the classes. Although this revealed a fair ability to separate the classes, it also showed that ptotic eyelids have much larger variances in the parameters than healthy eyelids – this implying that better results could be expected with a curved (rather than planar) surface separating the classes. This latter was achieved by using a Gaussian

classifier that involves calculating the means (μ_c) and covariance matrices (σ_c) for each class (c) and then assigning an eye with parameters *x* to class *c* with a probability.

$$p(c|x) = \frac{|2\pi\sigma_c|^{-1/2}\exp[-\frac{1}{2}(x-\mu_c)^T\sigma_c^{-1}(x-\mu_c)]}{\sum_c |2\pi\sigma_c|^{-1/2}\exp[-\frac{1}{2}(x-\mu_c)^T\sigma_c^{-1}(x-\mu_c)]}$$

[1]

In expression [1], as is conventional, || denotes a determinant and a superscript T denotes a transposed vector. Note that this assumes equal prior probabilities for all classes – that is, before any measurements are taken any eye is assumed to be equally likely to be healthy or ptotic.

3. Results and discussion

3.1 Palpebral aperture, blink duration and blink speed

The cinematographic PA in this study ranged from 1.15 to 10.45mm with a mean of 6.90 ± 0.30mm (standard error of the mean; hereafter abbreviated as SEM in text) in 26 ptosis patients; compared to the range of 6.29 to 12.78mm with a mean of 9.08 ± 0.15mm (SEM) of all 45 control subjects. Ptosis patients have a significantly smaller PA (P=0.003; table 1). These measurements were made during the high speed camera image analysis rather than being actual measurements on the volunteers. The PA master curve is shown in figure 1 & 2 for controls and ptosis patients.

Total blink durations were calculated from the start of upper eyelid descent until maximum recovery in each isolated blink in ptosis and the control subjects. Only 14/131 eyes did not achieve 100% recovery, of which 3 were from ptosis patients. The incompletely recovered blinks have a mean of 96.8% recovery, ranging from 79 to 99.7% across all subjects. Ptosis patients have average blink duration of 560 ± 50ms (SEM), greater than that of the control group; 530 ± 22ms (SEM) of the controls. However, while there was a trend for blinking duration in ptosis patients to be greater than controls, the data were not significantly different (p=0.28). A summary is presented in table 1, together with the peak speed achieved in ptosis and in control patients.

			Blinking dynamics (2 s.f.)		
References	**Number of test subjects**	**Age**	**Maximum velocity (mm/s)**	**Palpebral aperture (mm)**	**Duration (ms)**
(Kwon, et al., 2013) Controls	25	25-63	240±9	9.8±0.17	570±25
This study: Controls	20	29-67	290±16	8.2±0.18	490±40
Ptosis	26	22-84	260±14	6.9±0.30 *	560±50
Additional subjects	7	22-77	210±29	7.9±0.51	810±130

Table 1.| Results of upper eyelid blink dynamics from this study and Kwon et al.(13).

** indicates significantly different from the control subjects.*

Figures 1 & 2 show how the normalised PA changed over time, with the average speed overlay. They both share similar key features such as a rapid decrease in PA and then a slower and distinctively two-stage opening phase – after which they reach approximately

97% recovery, in agreement with Kwon *et al.* (13). The speed master curve exhibits two parabolic curves; one for the closing phase and the other one for the opening phase. In comparison, ptosis patients have very similar upper eyelid closure acceleration to the control group, with peak speed at near-mid closing and then decelerating until reaching their full closure. However, the initial opening speed (second parabolic speed curve) seems to have diminished in the ptosis patients compared to the controls. Ptosis patients have a mean peak speed of 258.7±13.7mm/s (SEM), (range 105.5 to 459.5mm/s) and the control subjects have 260±8.5mm/s (SEM) (range 128.5 to 482mm/s), with a significance of 0.79; thus, the null hypothesis of there being no difference between the two peak speed means was confirmed.

The speed of blink was then considered as two components in each subject: the closing phase and the opening phase (figure 4). During the closing phase, the peak speed in controls ranges from 130 to 480 mm/s (mean 260±9mm/s; mean±SEM), as compared to the ptosis group, ranging from 110 to 460mm/s (mean of 254±15mm/s; mean±SEM). Considering the opening phase as a single entity, the peak speed in the control group ranged from 90 to 260mm/s (mean of 156±4mm/s), compared to the ptosis group ranging from 50 to 375 (mean of 160±14mm/s; mean±SEM); figures were rounded to the nearest integer. These findings might suggest that altered intrinsic LPS muscle function has a role in the development of acquired ptosis, rather than dehiscence of the LPS from the tarsal plate, and might explain the long-observed feature of reduced eyelid excursion in acquired ptosis. However, the above SEM values of the ptosis group were insignificant compared to controls.

Whilst it was expected that the closing phase would always achieve higher speed than the opening phase, a small number of ptosis patients (4/26) achieved a faster upper eyelid

opening speed than closing. The reasons for this are unclear, but these data might suggest a more widespread motor dysfunction, extending to orbicularis function, presenting in patients with ptosis.

3.2 Distinctive two-stage recovery.

A characteristic two-staged PA recovery was observed in each individual PA *versus* time graph, indicated as 'switch point' in figure 3. The outcome of the Mathematica model was greatly improved after this parameter was introduced, compared to the beta tests without this 'switch point'. One possible explanation for this phenomenon may be the extensive internal connective tissues and the activation of different muscle fibres in the extraocular muscles. The LPS muscle consists of a mixture of muscle fibres with fast-twitch fibres similar to those seen in the global layer of the extraocular muscles and also unique slow-twitch fibre types. The singly innervated global/slow type accounts for about a third of this layer and has a high mitochondrial content and has a high fatigue resistance. The global/fast type, on the other hand, has a low mitochondrial content with low fatigue-resistance (18). These muscle fibres subtypes work in parallel with different functional properties, and this might explain the distinctive two-staged recovery during the opening phase of a blink.

The curved traces of the PA *versus* time graph during the initial closing and the latter opening phase is likely to be due to the muscle architecture. Most muscle fibres are short and do not extend to the tendons (19). The myofibres in each muscle are concentrated in the mid-section and decrease in density as they approach their insertions, contributing to the nonlinear contraction properties in the PA *versus* time graphs.

3.3 The effect of age

It was necessary to explore the possibility that the results of the present study are merely age-related effects rather than a true difference between the controls and the affected eyelids.

All normalised PA *versus* time graphs for the control subjects were plotted with their respective speed plot over-laid. All parameters were calculated and full details are provided in supplementary information 2. When the functions were applied to the individual eyelids, in order to have the best fit, some did not start at 100% due to the stepwise fitting of an initial constant PA followed by closing at a speed v_1, the rate at which the upper eyelid descends; an example of the fitting can be seen in figure 3. For example in supplementary information 2, subject ID 2C4 [left eyelid, LE], 2C33 [LE and right eyelid, RE] did not start at 100%, and it was noted that 63% of these subjects also have incomplete closure.

These data were analysed using LDA and before being separated into their respective age groups (≥40 and <40), there were some major overlaps. However, there was an obvious separation of the two means when divided into two groups (figure 5). Mahalanobis distance was used as the discriminant to measure how many standard deviations a data point is away from the mean of the distribution in a multidimensional space; the closer the distance to the centre of distribution, the more likely it is to belong to that class. The function used to describe this distance is defined as:

$$\sqrt{(x-\mu_c)^T \sigma_c^{-1} (x-\mu_c)} \qquad [2]$$

Symbols were defined before in equation [1].

A significantly large separation between the means of the two groups (figure 5) shows that age is a factor in blinking dynamics and that it would be appropriate to conduct further analysis with a group of controls selected to age-match the patients suffering from ptosis.

3.4 Ptosis versus control

It has been shown that age is a factor in blink dynamics and, to remove this effect in further analysis, we have compared the ptosis group with the control subjects aged ≥40. Using the same parameters as described above, all the PA *versus* time curves were reconstructed for all ptosis patients and the selected control subjects and the key features extracted (figure 6). The value of the minimum is only included if the eye closure was not complete. The start and end percentages were not included because they are not really shape parameters (full details are presented in supplementary information 3).

The three-dimensional display (figure 6) was reduced to generate figure 7. There is a clear difference between the class means, but there are still overlaps in the middle portion. A probability-based discriminant was used to differentiate between the two classes because the data are differently spread in the classes. Therefore a dividing curve that curls around the class that is less widely spread out is better to separate the two of them: a linear discriminant function leading to a planar separation was inadequate in this case.

A slower rate of eye opening in ptosis patients compared to controls, characterised by v_2 was observed and therefore a more quantitative measurement was sought. A histogram was generated for comparison of the v_2 parameter between the ptosis patients (mean of 0.87 with the variance of 0.108), and controls (mean of 1.01 with the variance of 0.057). Figure 8 demonstrates a heavy overlap between the two sets of data but Mann-Whitney tests have revealed a significant difference in the mean at the p=0.005 level. Although this

might serve as an indicator for distinguishing ptosis from controls, one must note that this is just one of the features used in the discriminant process and would not be sufficient for diagnostic purposes.

This analysis gives us a model to discriminate ptosis from normal cases and this data-set constituted the 'learning' set of data. The discriminant can be applied to a new set of untested subjects, and hence a further test-set of seven additional subjects was acquired to investigate the robustness of the procedure (table 2).

ID	Probability for normal	Probability for ptosis	Model prediction		Clinical diagnosis
1-19 [LE]	0.10	0.90	Ptosis	√	Ptosis
1-19 [RE]	0.00	1.00	Ptosis	√	Ptosis
1-23 [LE]	1.00	0.00	Normal	X	Ptosis
1-23 [RE]	1.00	0.00	Normal	√	Normal
1-24 [LE]	1.00	0.00	Normal	√	Ophthalmoplegia
1-24 [RE]	0.65	0.35	Normal	√	Ophthalmoplegia, myopathy (worst side)
1-25 [LE]	0.22	0.78	Ptosis	√	Ptosis
1-25 [RE]	0.01	0.99	Ptosis	√	Ptosis
1-37 [LE]	1.00	0.00	Normal	X	Ptosis
1-37 [RE]	1.00	0.00	Normal	√	Normal
1-6 [LE]	1.00	0.00	Normal	√	Normal
1-6 [RE]	1.00	0.00	Normal	X	Traumatic Ptosis
1-7 [LE]	1.00	0.00	Normal	√	Tarsorrhaphy
1-7 [RE]	1.00	0.00	Normal	√	Normal

Table 2.| Probability test for the 7 additional test subjects (in 2 decimal places). This group of subjects has all been assumed to have ptosis for the purpose of this exercise and after applying our model on Mathematica, 4 out of 6 eyes were correctly considered ptotic; 10

cases were considered normal of which, 3 cases were misclassified. Correct prediction from the model was represented by tick marks on the right and misclassification by cross marks.

In Table 2, ID 1-19 [LE] achieved 90% of certainty as a ptosis subject whereas it's [RE] counterpart is 100% ptosis, and ID 1-25 [LE] was predicted 78% and [RE] 99% for ptosis; both of these match with the clinical diagnosis. However, the model failed to pick up ID 1-23 [LE], 1-37 [LE] and 1-6 [RE] as ptosis and considered them normal. An interesting case here is that ID 1-6 [RE] has traumatic ptosis, a physical injury that causes reduced function of the upper eyelid. It is likely that the reason the present model failed to classify it as ptosis is that the causation of the ptosis was an injury rather than a developed disease, such as neurological or aponeurotic. There are no cases of traumatic ptosis in our learning set of data.

ID 1-24 [LE] & [RE] and 1-7[RE] in Table 2 have been classified as normal and the clinical diagnosis is of ophthalmoplegia and tarsorrhaphy, respectively. The present model was programmed to detect ptosis, and therefore other diseases are likely to be classed as 'normal': this does not mean they are completely healthy. Note ID 1-24 [RE] in Table 2 achieved 65%/35% as normal/ptosis, suggesting some abnormality or borderline ptosis. This was understandable as the patient has been diagnosed with myopathy, ocular muscle paralysis, and this right eye is the worse of the two eyes. Other normal cases (Table 2) have been correctly classified as normal, such as ID 1-23 [RE], 1-37[RE], 1-6 [LE] and 1-7 [RE].

3.5 Future developments

Our model failed to diagnose the one instance of ptosis caused by trauma, having predicted 0% probability for ptosis for case 1-6 [RE] (Table 2). It might also be insensitive to weakness and atrophy of ocular muscles from myopathies or paralysis. With more sophistication this model has the potential to predict specific causations of ptosis with relatively good accuracy. On the other hand the type of blinking captured in the high-speed recordings may be a factor. It is possible that even clinically-diagnosed ptosis patients may have some aspect of blinking dynamics that are comparable to controls. This is an aspect that could be investigated further.

On fitting models, not all PA *versus* time curves have been matched as tightly as they could be. For example in figure 9, the starting point has been replaced by a kink in a piece-wise linear function, but the original trace has a smoother shape. Similarly some curvature was seen in a small section just before full closure and at the beginning of the opening phase. For future improvements, a function could be designed with extra parameters that could also capture these minute, but possibly significant features. Furthermore, we could introduce the severity of the ptosis as an extra parameter to improve the 'learning' in the present model.

4. Conclusions

Resting maximum PAs in ptosis patients were significantly lower than those of controls and ptosis patients also had a greater range of PA (1.15-10.45mm, compared with 6.29-12.78mm in controls). The average duration of a single blink in ptosis patients was

560±24ms (SEM), a small but statistically insignificant increase from the 530±22ms (SEM) of the controls.

The speed master curve in control subjects exhibit two parabolic curves; one for the closing phase and the other for the opening phase, with the peak speed of 260.0±8.5mm s^{-1} (SEM). However in ptosis patients, this curvature during the initial opening phase was reduced, demonstrating a much lower rate of recovery during opening phase. The speed curve in the PA *versus* time plot could also be the combined effect of LPS, Müller's muscle, frontalis muscle and other accessory muscles. Therefore a reduced rate of opening/ acceleration at the initial opening phase was observed. Peak speeds were found to be 258.7±13.7mm s^{-1} (SEM), both peak speed and range were very similar between the two groups. Not all subjects achieved higher closing speeds as compared to opening: 4 subjects, all with ptosis, had faster opening of the upper eyelid – all within the first 50ms after opening phase was initiated.

The analysis in this study showed a significant separation in PA between the control subjects of age ≥40 and those <40. Recognising that age is a factor statistically, the ptosis group was compared with the control with subjects aged ≥40. Using some of the key features of the blinking profile, PA *versus* time curves were reconstructed for each subject. A model was generated using these data and was able to discriminate ptosis from a set of data with good accuracy.

An additional seven subjects (14 eyes) were used to test the model's robustness and achieved 11/14 (80%) successful predictions, discriminating ptosis from controls. At present this model is not sensitive to traumatic ptosis, nor is it sensitive to weakness and atrophy of ocular muscles from myopathies or paralysis. In future developments of this model, it would

be beneficial to add more ptosis and control cases into the learning data set and thereby improve accuracy.

5. Acknowledgements

This work benefitted from the financial support from UCL (IMPACT Studentship) and Moorfields Eye Hospital NHS Foundation Trust. Staff from Moorfields Eye Hospital were gratefully acknowledged for their help and support. DGE and GER acknowledge Department of Health funding through the National Institute for Health Research to Moorfields Eye Hospital NHS Foundation Trust and UCL Institute of Ophthalmology for a Specialist Biomedical Research Centre for Ophthalmology. The authors wish to thank the Engineering and Physical Sciences Research Council, UK for providing the Phantom camera for this work. The generous help of Adrian Walker of the Instrument Loan Pool is gratefully acknowledged. The authors thank Dr. Maryam Parhizkar for her help with the high-speed camera. In addition, thanks are due to the staff of Moorfields NIHR clinical research facility and to Mr Ed White for extending the facilities to undertake this work.

References

1. Sudhakar P, Vu Q, Kosoko-Lasaki O, Palmer M. Upper Eyelid Ptosis Revisited. Amer J Clin Med. 2009;6(3):5-14.
2. Le TT, Farkas LG, Ngim RCK, Levin LS, Forrest CR. Proportionality in Asian and North American Caucasian Faces Using Neoclassical Facial Canons as Criteria. Aesthetic Plastic Surgery. 2002;26(1):64-9.
3. Dortzbach RK, Sutula FC. Involutional Belpharoptosis. A Histological Study. Archives of ophthalmology (Chicago, III:1960). 1980;98(11):2045-9.
4. Fujiwara T, Matsuo K, Kondoh S, Yuzuriha S. Etiology and Pathogenesis of Aponeurotic Blepharoptosis. Ann Plast Surg. 2001;46(1):29-35.
5. Paris GL, Quickert MH. Disinsertion of the Aponeurosis of the Levator Palpebrae Superioris Muscle After Cataract Extraction. American Journal of Ophthalmology. 1976;81(3):337-40.
6. Orchard L, Stern J. Blinks as an Index of Cognitive Activity During Reading. Integration Physiology and Behavioural Science. 1991;26(2):108-16.
7. Radlak K, Smolka B. A novel approach to the eye movement analysis using a high speed camera. 2nd International Conference on Advances in Computational Tools for Engineering Applications (ACTEA)2012. p. 145-50.
8. Castro F. Class I Infrared Eye Blinking Detector. Sensors and Actuators A: Physical. 2008;148(2):145-50.
9. Evinger C, Manning K, Sibony P. Eyelid Movements: Mechanisms and Normal Data. Investigative Ophthalmology & Visual Science. 1991;32(2):384-400.
10. Korošec M, Zidar I, Reits D, Evinger C, VanderWerf F. Eyelid Movements During Blinking in Patients With Parkinson's Disease. Movement Disorder. 2006;21:1248-51.
11. Sun W, Barker J, Chuke J, Rouholiman B, Hasan S, Gaza W, et al. Age-related Changes in Human Blinks. Investigative Ophthalmology & Visual Science. 1997;38:92-9.
12. VanderWerf F, Brassinga P, Reits D, Aramideh M, de Visser B. Eyelid Movements: Behavioural Studies of Blinking in Humans Under Different Stimulus Conditions. Journal of Neurophysiology. 2003;89(5):2784-96.
13. Kwon KA, Shipley R, Edirisinghe M, Ezra D, Rose G, Best S, et al. High-Speed Camera Characterization of Voluntary Eye Blinking Kinematics. Journal of the Royal Society Interface. 2013;10.
14. Fox SA. Ophthalmic Plastic Surgery. 5th ed. New York: Grune & Stratton; 1976.
15. Nerad JA. Techniques in Ophthalmologic Plastic Surgery. 1 ed: Cincinnati. Saunders Elsevier; 2010.
16. Salouti R, Nowroozzadeh M, Zamani M, Salouti R. Comparison of Horizontal Corneal Diameter Measurements Using Galilei, Eyesys and Orbscan II Systems. Clinical and Experimental Optometry. 2009;92(5):429-33.
17. Bishop C. Discriminant Functions. Pattern Recognition and Machine Learning. New York: Springer International Edition; 2006. p. 186-92.
18. Porter J, Burns L, May P. Morphological Substrate for Eyelid Movements: Innervation and Structure of Primate Levator Palpebrae Superioris and Orbicularis Oculi Muscles. Journal of Comparative Neurology. 1989;287(1):64-81.
19. Harrison A, Anderson B, Thompson L, McLoon L. Myofiber Length and Three-Dimensional Localization of NMJs in Normal and Botulinum Toxin Treated Adult Extraocular Muscles. Investigative Ophthalmology & Visual Science. 2007;48(8):3594-601.

Figures

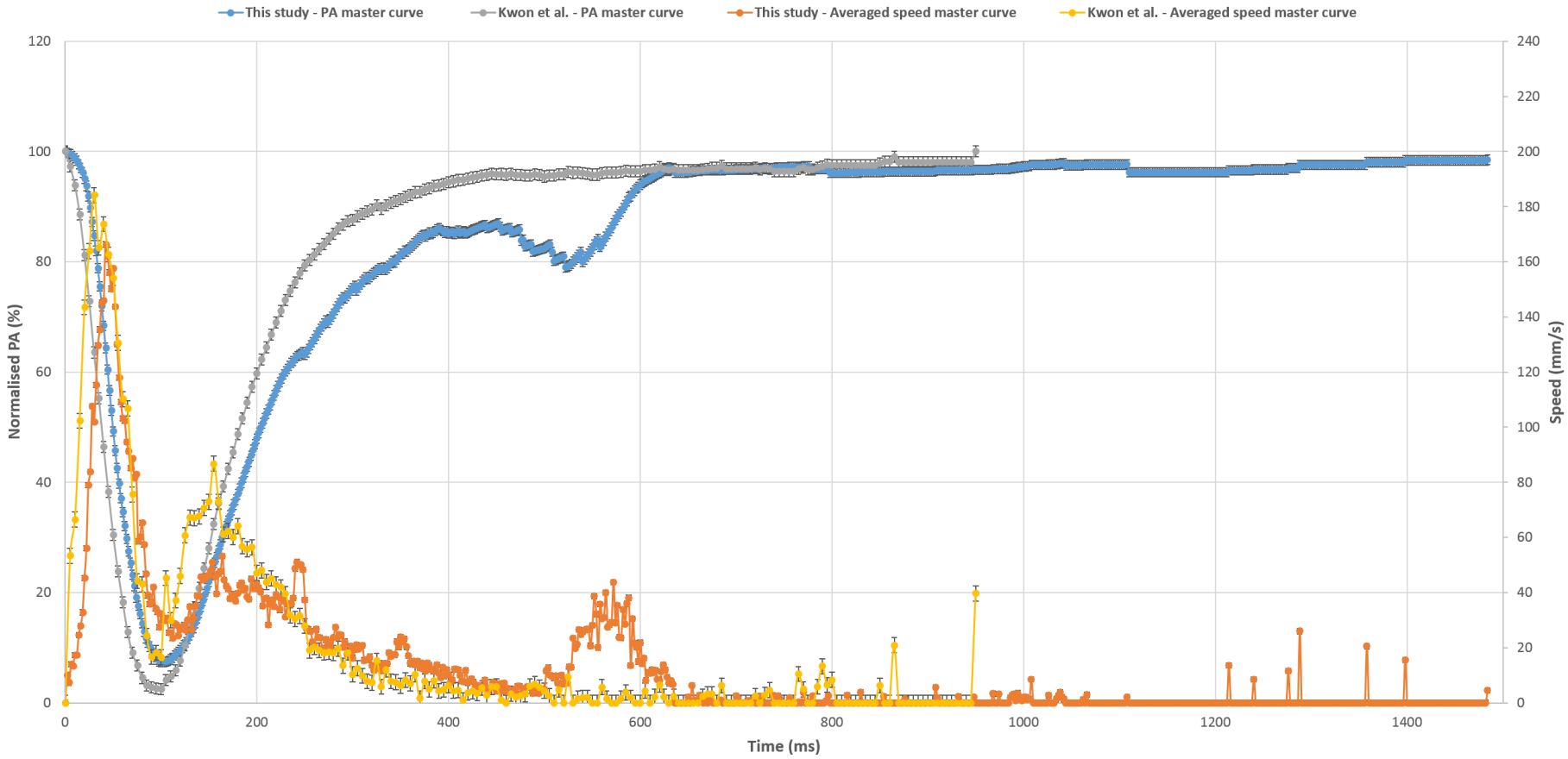

Figure 1.| PA and speed master curves for all controls. Two sets of normal subject's blinking: Kwon *et al.* 2013 palpebral aperture master curve is shown in grey and its respective speed is shown in yellow (13). The palpebral aperture master curve is shown in blue and its respective speed is shown in orange. Secondary axis for the speed master curve is on the right hand side, measured in mm/s. The chart is plotted with mean±SEM.

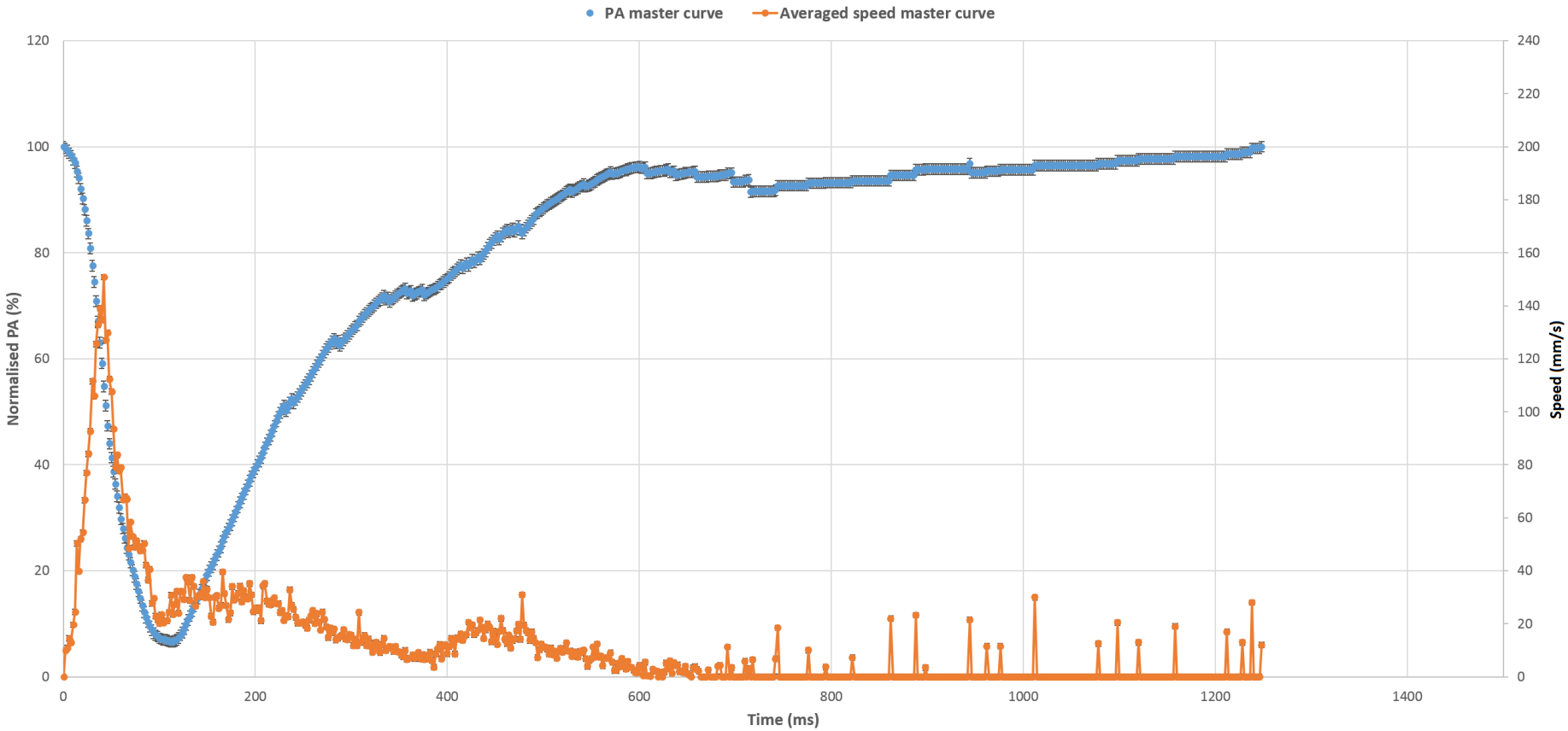

Figure 2.| PA and speed master curves for ptosis patients. Palpebral aperture vs speed master curve for both left and right eyes in ptosis patients. The palpebral aperture master curve is shown in blue and its respective speed is shown in orange. Secondary axis for the speed master curve is on the right hand side, measured in mm/s. The chart is plotted with mean±SEM.

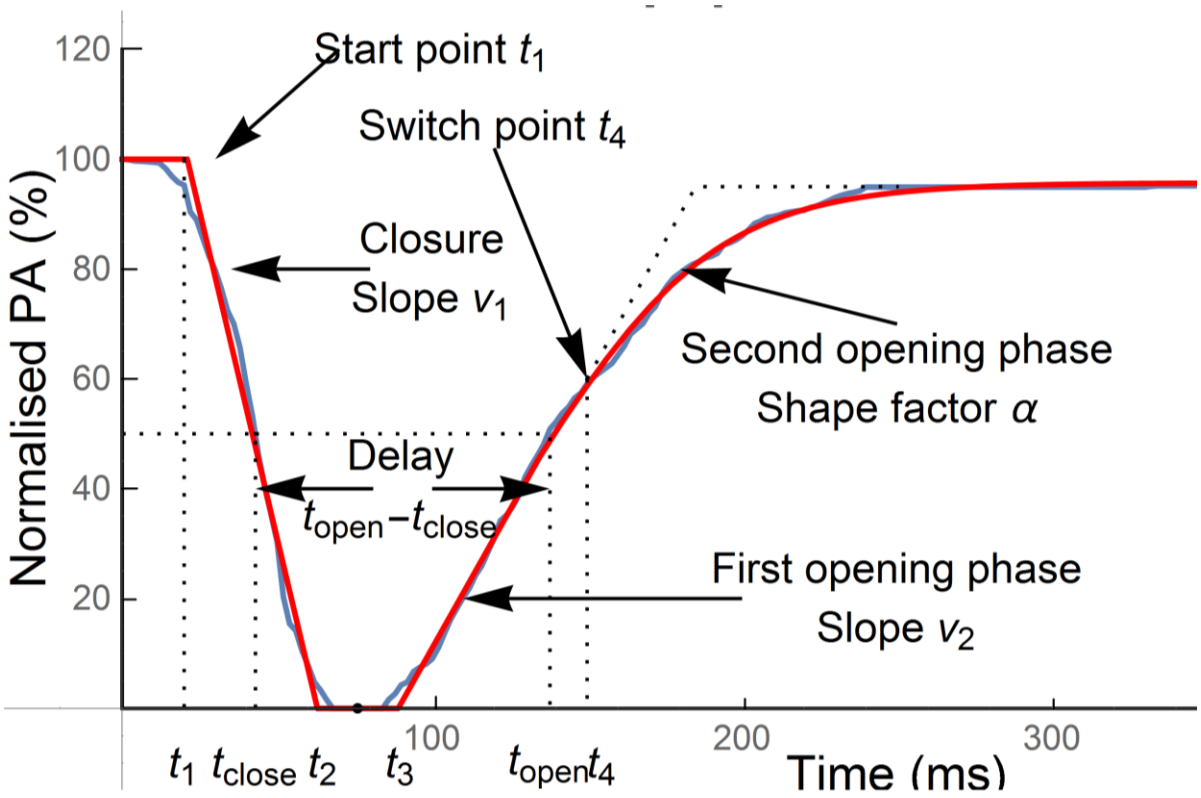

Figure 3.| Fitting the blinking profile. An example of breaking down the blink PA vs time curve into possible key features – parameters that could be used in our analysis. The blue trace is the PA measurement against time, and the red trace is fitting of the functions designed to represent the key features of the blink profile.

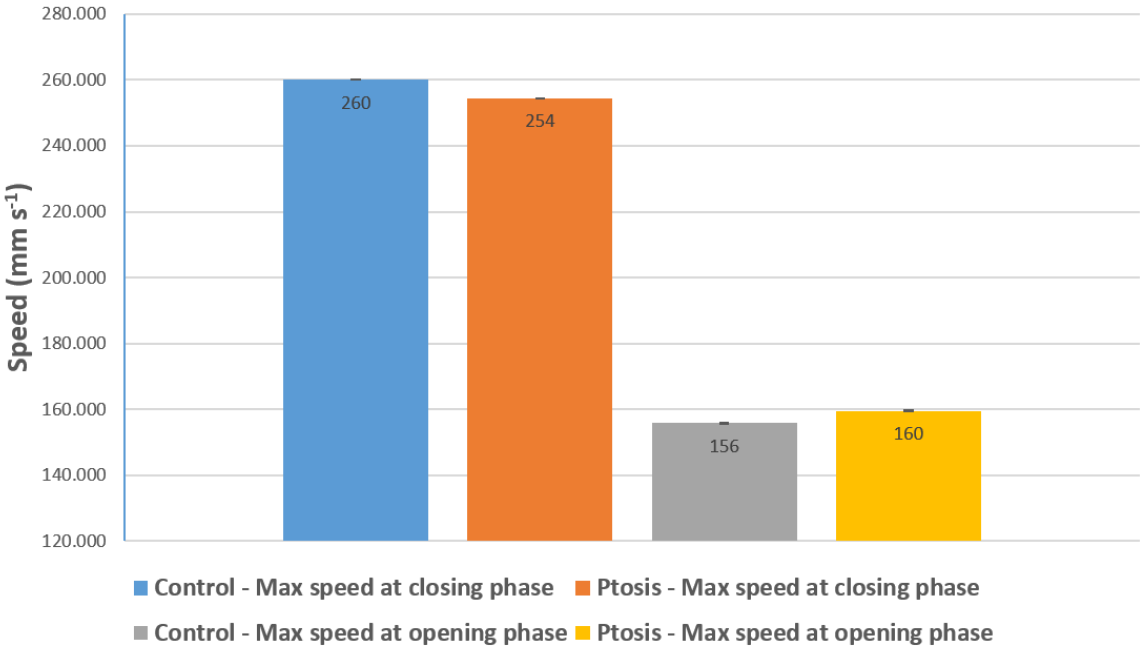

Figure 4.| Maximum speed during opening and closing phases: control vs ptosis (to the nearest number). The bars represents the averaged maximum speed during different phases of blinking: Blue is control closing compared to orange for ptosis closing; and grey is control opening comparing to yellow for ptosis opening. Error bars are shown as SEM.

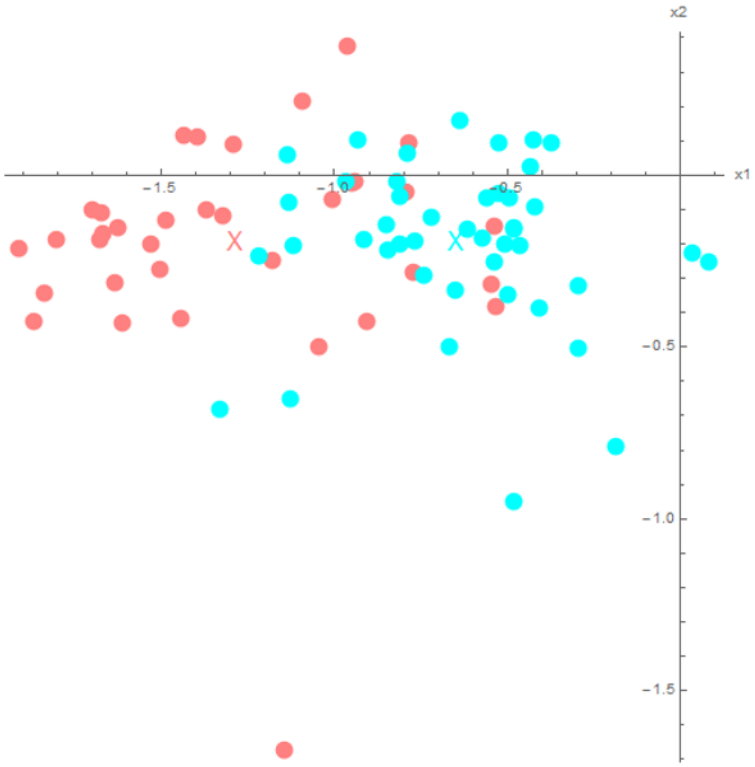

Figure 5.| Blinking discriminant between control subjects of ≥40 (pink) vs <40 (cyan). This analysis used the 5 parameters mentioned in the text: rate of closure, delay between opening and closing, initial rate of opening, switch point and rate of slow opening. The coloured X is the mean of the respective group. Values on x1 and x2 axes are merely numbers representing the reduced dimension in LDA.

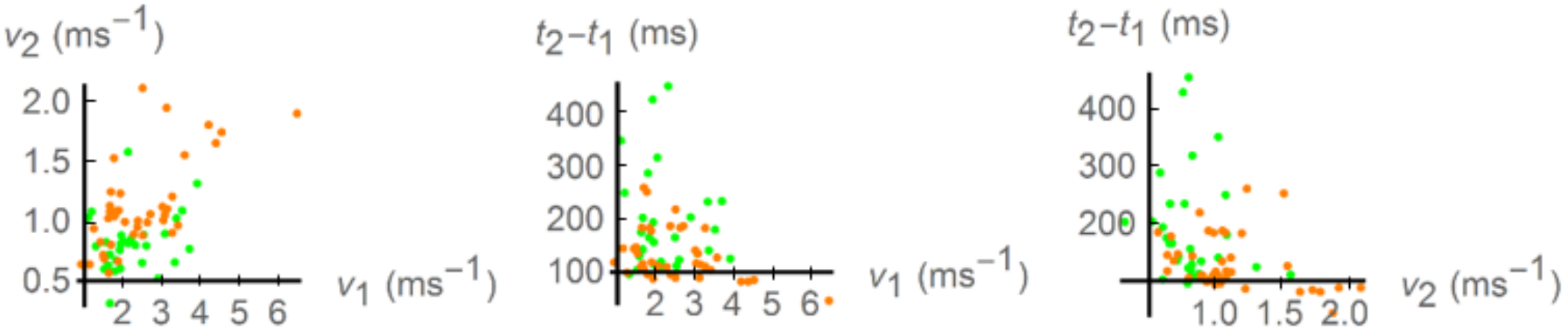

Figure 6.| Three dimensional discriminant display of the parameter used for ptosis (all ages; green) and controls (≥40year-old; orange). v_1, v_2 t_{open} and t_{close} are defined in text (section 2.5). The value of min is neglected as it does not have much significance, as the real value of the minimum is often at a cusp. Also the start and end % were not considered because they are not really shape parameters.

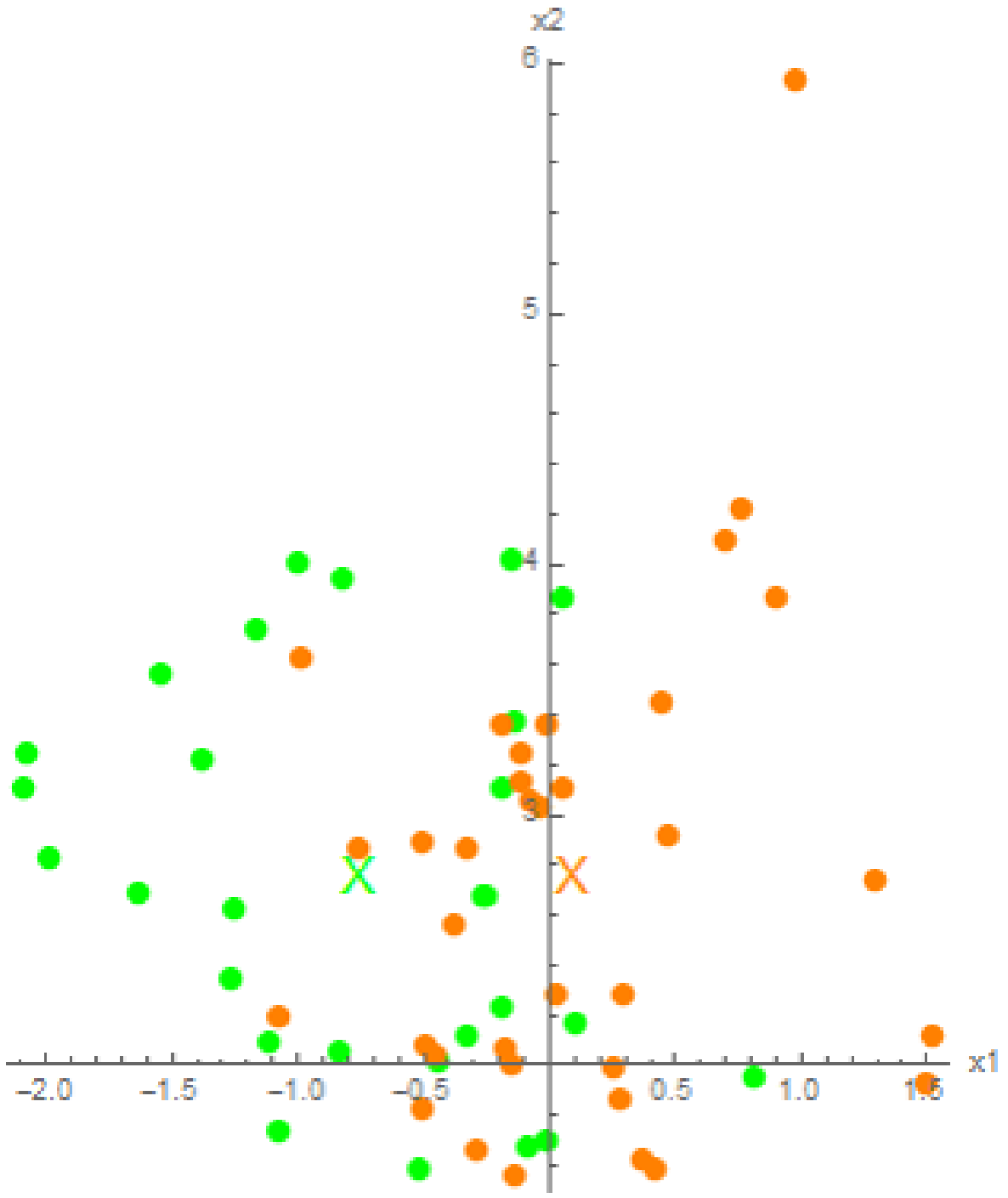

Figure 7.| Ptosis patients (green) vs ≥ age 40 controls (orange) in the reduced dimension of the linear discriminant. Axes x1 and x2 are the first two principal directions in the space of the linear discriminant. The class means are shown as the X marker in its respective colour.

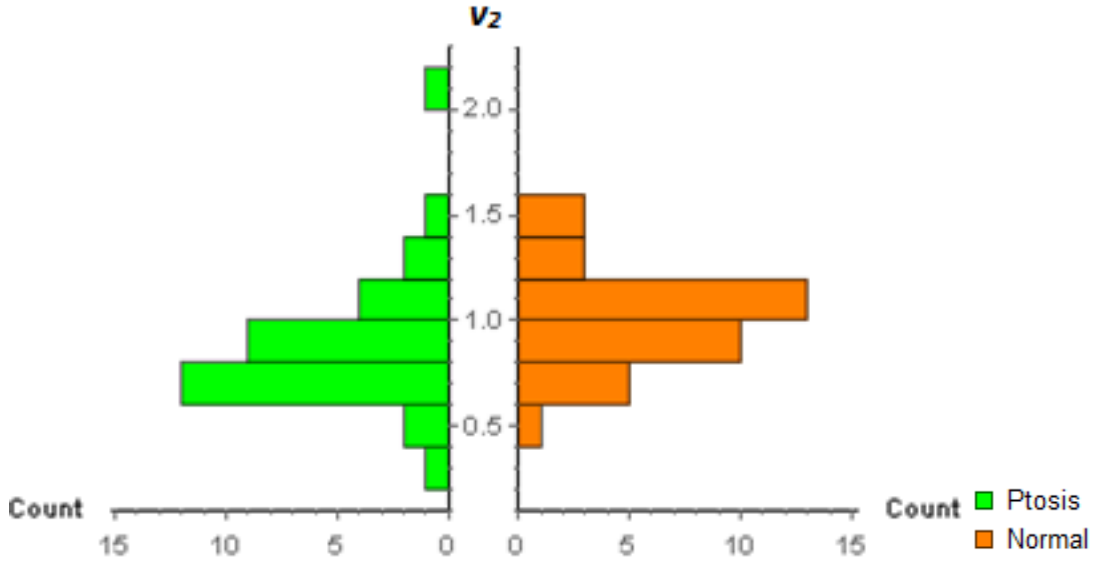

Figure 8.|Comparison of v_2 parameter between ptosis and control patients are displayed on this histogram. It demonstrates a slower rate of opening in the ptosis patients than the controls by a small, but significant amount.

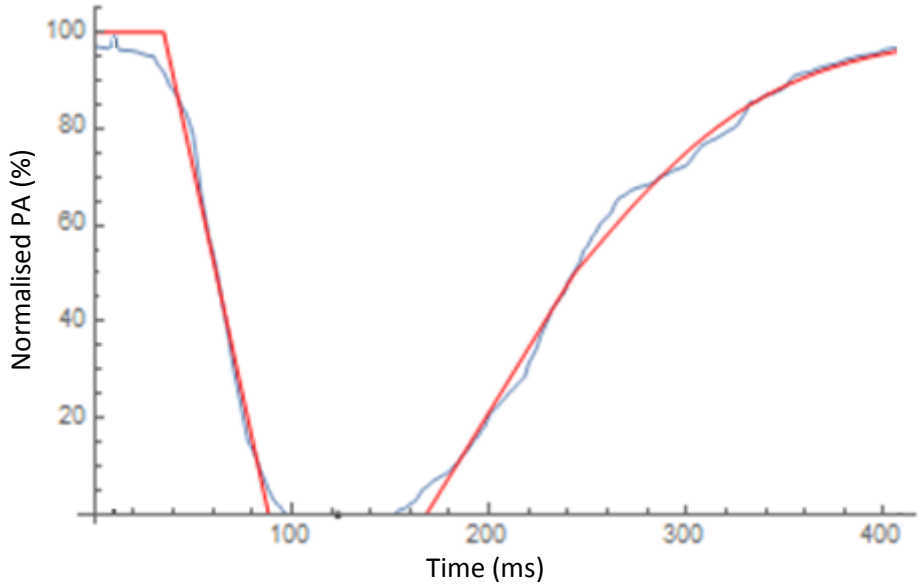

Figure 9.| Fitting of the blinking profile on the PA vs time curve for a control patient. It is clear that the blinking profile is not fitting every detail if we only have linear functions for closure and initial opening. Some of the information is lost after conversion into the fitting function.

There were 18 aponeurotic ptosis: 10 cases of primary surgery for aponeurotic ptosis correction (2 of then due to long standing use of contact lens and 8 was age related involutional ptosis); 8 cases of redo aponeurotic ptosis correction (1 case ptosis induced by cataract surgery in childhood, 1 case of long standing contact lens, 6 cases age related involutional ptosis).

2 case of TED ptosis induced by over correction of previous lowering upper lid surgery (both cases were a redo ptosis correction).

1 case of III nerve palsy with aberrant degeneration.

2 case of ptosis in an ophthalmic socket.

1 case of VII nerve palsy ptosis

1 case related to parathyroidectomy surgery.

1 case of Horner syndrome surgically induced following a sympathectomy.

Supplementary information 1.| Breakdown of causations of diseased patients included in this study.

ID	blink	start%	toff	min	sharp1	ton	ton-toff	sharp2	tswtch-ton	sharp3	end%	R^2
2C17[LE]		100	33.2221	0.	2.27126	142.476	109.254	0.891468	3.38638×10^{-7}	0.571265	97.8808	0.999623
2C17[RE]		100	43.8741	8.92483	1.68244	149.228	105.354	0.802713	1.13574×10^{-7}	0.446368	94.9334	0.999687
2C4[LE]		97.5162	90.8913	3.48361	1.25145	189.261	98.3694	0.940935	1.6006×10^{-6}	0.505924	100	0.999517
2C4[RE]		100	61.2854	28.8092	0.921826	178.973	117.687	0.637487	0.0036132	0.460459	98.1354	0.999798
2C33[LE]		98.58	54.6811	8.17918	1.78487	150.	95.3189	1.04477	1.88402	0.844755	100	0.99974
2C33[RE]		98.2616	50.5809	0.	2.0516	162.	111.419	0.994389	1.91753	0.825754	100	0.999455
2C1[LE]		100	37.5596	0.	3.1343	151.632	114.072	1.10628	2.24223×10^{-7}	0.480797	98.768	0.999727
2C1[RE]		100	31.8765	0.	3.03873	148.37	116.494	1.00877	0.000450977	0.478152	99.2113	0.999779
2C14[LE]		100	38.6147	0.	3.12388	161.34	122.725	1.1533	4.41675×10^{-7}	2.14341	46.7715	0.708034
2C14[RE]		100	39.8133	0.	3.0232	370.166	330.353	1.49933	-12.1658	1.15636	100	0.800533
2C21[LE]		100	55.1889	0.	1.636	240.	184.811	0.565761	6.38691	0.489616	95.2213	0.995631
2C21[RE]		100	61.7127	0.	1.87946	240.	178.287	0.666018	3.19383	0.486443	100	0.998445
2C25[LE]		100	30.7238	0.	3.26855	141.213	110.49	0.903975	1.24019	0.421698	97.0898	0.99965
2C25[RE]		100	31.3882	0.	3.41929	134.899	103.51	0.964235	0.0685733	0.648443	95.0825	0.999245
2C19[LE]		100	73.9889	0.	1.83591	258.	184.011	1.08525	0.325704	0.650381	100	0.999234
2C19[RE]		100	66.8889	0.	2.50687	286.383	219.494	0.883623	-3.72443	0.617905	98.7569	0.999254
2C23[LE]		100	33.3248	0.	3.58356	160.058	126.733	1.5588	0.866968	0.784379	98.3606	0.999428
2C23[RE]		100	33.4866	0.	3.01685	174.287	140.8	1.12255	-0.0535409	0.488282	99.7782	0.999482
2C43[LE]		100	57.2818	0.	1.42325	201.09	143.809	0.828008	-2.52639×10^{-6}	0.495425	95.4098	0.999666
2C43[RE]		100	59.0504	0.	1.51795	194.175	135.124	0.68507	-34.6442	0.696192	96.0598	0.99987
2C45[LE]		100	46.6449	0.	2.62463	231.15	184.505	0.992585	-6.05824	0.695693	98.3672	0.999603
2C45[RE]		100	52.8357	0.	2.36925	240.627	187.791	0.951203	0.461962	0.608289	98.8019	0.999413
2C6[LE]		98.3098	84.3831	6.51163	1.14438	229.547	145.164	0.638655	3.56948×10^{-6}	0.304058	99.6744	0.999658
2C6[RE]		100	54.0414	0.	1.48616	201.098	147.057	0.719199	1.41229×10^{-8}	0.421515	96.5757	0.999591
2C29[LE]		100	56.9382	0.	1.65816	172.201	115.263	1.12936	0.307515	0.823138	100	0.998426
2C29[RE]		98.2791	49.9313	11.1617	1.62348	160.	110.069	1.02575	1.20728	0.771417	100	0.999038
2C39[LE]		100	53.893	0.	1.68384	314.791	260.898	1.24794	0.00901198	0.577062	97.4634	0.999591
2C39[RE]		100	52.5141	0.	1.77131	305.198	252.683	1.52941	5.52808×10^{-6}	0.489305	96.8735	0.99953
2C7[LE]		100	38.3804	0.	3.27081	221.876	183.496	1.20854	6.06359×10^{-7}	0.828223	97.8826	0.999593
2C7[RE]		100	42.1174	0.	2.70323	229.717	187.6	1.06048	0.0410156	0.641394	100	0.999292
2C11[LE]		100	43.8943	3.51938	1.93051	130.484	86.5893	1.23727	0.216807	0.602812	97.6113	0.999628
2C11[RE]		100	41.9903	0.	2.3819	136.	94.0097	1.00279	0.759684	0.841814	95.6891	0.999539
2C27[LE]		100	65.3627	0.	1.65635	170.	104.637	1.08485	0.848051	0.850493	100	0.999141
2C27[RE]		97.6499	58.2535	0.	1.89224	176.	117.747	1.0902	0.83895	0.746385	100	0.999536
2C31[LE]		100	88.0966	0.	3.07867	223.132	135.035	1.0547	-3.05043	0.804619	100	0.999667
1C17[LE]		100	39.6943	0.	1.67966	243.372	203.678	0.724414	0.543073	0.389829	96.603	0.999329
1C17[RE]		100	33.4965	0.	1.81425	245.236	211.74	0.700388	0.0000132798	0.35635	96.8625	0.999158
1C4[LE]		100	89.9999	0.	1.25	311.16	221.16	0.782197	0.0551384	0.622711	100	0.997566
1C4[RE]		100	84.7593	0.	1.00213	305.	220.241	0.848365	2.96477	0.534057	100	0.997588
1C11[LE]		100	36.4342	0.	2.29251	141.394	104.96	0.629395	10.545	0.586968	96.2694	0.99931
1C11[RE]		100	33.5536	0.	2.58875	145.195	111.641	0.761879	1.60185×10^{-6}	0.515101	97.0299	0.999492
1C3[LE]		100	37.9166	0.	1.75619	241.642	203.725	0.662424	-4.82031×10^{-6}	0.336546	96.551	0.999524

ID	blink	start%	toff	min	sharp1	ton	ton-toff	sharp2	tswtch-ton	sharp3	end%	R^2
2C3[LE]		98.7789	55.7812	18.4312	0.976381	291.966	236.185	0.403157	-66.7096	0.908702	100	0.998883
2C3[RE]		100	60.5286	0.	1.30547	286.	225.471	0.841404	1.46327	0.817869	98.2011	0.999633
2C9[LE]		100	87.1258	0.	0.619471	580.617	493.491	0.498745	-24.0745	1.4658	100	0.983896
2C9[RE]		100	62.6204	2.27962	1.00009	552.	489.38	0.728894	3.53897	1.34438	100	0.979362
1C14[LE]		100	38.8959	0.	1.61895	149.218	110.322	0.934634	8.57101×10^{-8}	0.760007	100	0.999609
1C14[RE]		100	38.7413	0.	1.70884	151.342	112.601	0.929893	1.05234×10^{-6}	0.703858	100	0.999374
1C19[LE]		100	37.1739	0.	1.79365	133.082	95.9084	1.51255	1.1274×10^{-6}	0.46825	93.3907	0.999705
1C19[RE]		100	38.7137	0.	1.90453	137.635	98.9216	1.06242	-1.46246×10^{-6}	0.460048	93.7922	0.99936
1C23[LE]		100	46.5627	0.	1.31611	179.703	133.14	0.702856	3.84566	0.908607	96.8043	0.99963
1C23[RE]		100	40.4948	0.	1.34763	169.307	128.812	0.880262	-3.85497	0.73829	97.9125	0.999245
1C13[LE]		98.1131	33.8215	0.	1.99885	153.824	120.003	1.4396	-2.7175×10^{-7}	0.743258	100	0.999068
1C13[RE]		100	30.2432	0.	1.90724	159.94	129.697	1.19578	0.171968	0.524323	100	0.99968
1C18[LE]		100	34.123	0.	2.22523	145.999	111.876	0.96759	1.13385	0.560937	96.1897	0.999545
1C18[RE]		100	38.4717	0.	2.00128	138.973	100.501	1.15664	0.0000154144	0.632474	96.8227	0.999724
1C26[LE]		100	42.097	0.	1.27146	172.895	130.798	0.961107	1.74531	0.696974	97.8363	0.99957
1C26[RE]		100	45.0411	0.	1.17084	168.8	123.759	1.09411	-32.7178	0.979436	96.6319	0.99953
1C29[LE]		100	33.379	0.	1.61863	166.144	132.765	1.02243	5.19105×10^{-7}	0.61	97.5402	0.999702
1C29[RE]		100	32.9711	0.	1.68499	165.	132.029	0.93273	1.75596	0.577591	98.112	0.999544
1C27[LE]		100	42.2076	0.	1.25778	215.397	173.189	0.697242	-24.4412	0.969226	96.283	0.999612
1C27[RE]		100	43.8912	0.	1.32285	204.551	160.66	0.801544	-16.1862	0.756635	95.256	0.999551
1C33[LE]		100	45.1114	0.	1.56186	147.251	102.139	1.27801	2.14028×10^{-7}	0.500041	97.6648	0.999518
1C33[RE]		100	36.5469	0.	1.83971	145.913	109.367	1.31362	-9.33384	0.641479	97.3577	0.999732
1C22[LE]		100	42.9269	0.	1.41846	179.086	136.159	0.846792	2.96005×10^{-6}	0.368497	97.3816	0.999612
1C22[RE]		100	35.6257	0.	1.35472	172.47	136.845	1.02129	1.18622×10^{-6}	0.342688	97.5292	0.999403
1C6[LE]		100	43.2193	0.	1.98748	163.953	120.734	0.805678	6.85561×10^{-6}	0.409538	93.1493	0.99884
1C6[RE]		100	41.8206	0.	1.83617	151.839	110.018	0.958252	-1.62638×10^{-6}	0.270713	100	0.998207
1C15[LE]		100	41.7726	0.	1.47325	158.62	116.847	1.05586	-1.55792×10^{-6}	0.549295	97.8623	0.999738
1C15[RE]		100	39.1308	0.	1.43614	157.003	117.873	1.14095	1.27203×10^{-6}	0.415841	98.9852	0.999799
1C24[LE]		100	41.8316	0.	1.29006	191.351	149.519	0.849861	8.10975	1.46383	100	0.999109
1C24[RE]		100	41.8344	0.	1.27319	193.951	152.117	0.868174	-22.0629	1.46044	97.4715	0.999266
1C25[LE]		100	38.5226	0.	1.2473	175.102	136.579	1.05957	-40.1015	0.992079	96.4205	0.999395
1C25[RE]		100	36.9686	0.	1.40018	171.735	134.766	1.1179	0.715391	0.598322	96.7475	0.999573
1C32[LE]		100	45.0391	0.	1.05775	184.245	139.206	0.820004	0.0366348	0.893446	100	0.99944
1C32[RE]		100	50.724	0.	1.14964	174.036	123.312	0.979283	3.23329	1.02608	100	0.999449
1C16[LE]		100	39.6214	0.	1.95492	148.294	108.672	0.965934	4.62835×10^{-6}	0.389442	100	0.997368
1C16[RE]		100	42.3248	0.	1.82713	130.978	88.6537	1.44761	0.917278	0.62938	95.407	0.999351
1C9[LE]		100	26.0094	0.	2.60262	144.13	118.121	1.16382	3.15728	1.07914	100	0.998985
1C9[RE]		100	26.1296	0.	2.99499	141.496	115.366	1.21164	1.16588	1.09058	100	0.999089
1C8[LE]		100	37.3607	0.	1.76059	174.848	137.487	1.42648	-2.43325	0.808568	100	0.999533
1C8[RE]		100	35.5805	0.	1.87452	170.	134.42	1.57893	2.05634	0.884057	98.2697	0.99952
1C20[LE]		100	48.0826	0.	1.50689	244.511	196.428	0.720256	0.282954	0.428746	98.506	0.99899
1C20[RE]		100	43.6292	0.	1.39165	253.047	209.418	0.576918	-28.0472	0.834081	97.565	0.999766
1C21[LE]		100	34.191	0.	1.5384	168.842	134.651	1.24646	0.0340954	0.747187	98.2075	0.999498
1C21[RE]		100	33.3826	0.	1.67029	159.106	125.724	1.49692	1.21643×10^{-6}	0.991595	95.7101	0.999373
1C30[LE]		100	33.6227	0.	1.4406	216.962	183.339	0.552403	-22.2092	0.7582	96.371	0.99943
1C30[RE]		100	34.9997	0.	1.33497	229.981	194.981	0.469768	-77.7823	0.704274	92.8435	0.998557

Supplementary information 2.| Details of subjects *Left* Control subjects in the ≥40 group. *Right* Control subjects for the <40 years group. Start% = starting PA (normalised); toff = Time offset at half of closure; min = minimum PA; sharp1 (v_1)= rate of closure; ton = time onset at half initial opening; ton-toff = (t_{off}-t_{on}), time between half closing and half opening; tswitch-ton = (t_4-t_{open}), time delay from half opening to time of switch; sharp2 (v_2)= rate of initial opening; sharp3 (α)= shape parameter of late opening; end% = % of full recovery from start%.

Type	Case		sharp1	sharp2	ton – toff	tswitch – ton	sharp3
"Ptosis"	"2 – 49[RE]"	""	3.3686773759788 06	1.0273712786544358	141.32391508581355	1.0979057504223704	0.6958563033930171
"Ptosis"	"2 – 24[LE]"	""	2.900216369206696	0.5214602711867842	204.0046854882641	−19.66930493837708	0.34082390006851243
"Ptosis"	"2 – 26[LE]"	""	1.0950982608233455	1.0301143850649996	351.356160400036	0.510065830765484	0.7338379451237389
"Ptosis"	"2 – 14[LE]"	""	1.9315139384408515	0.6032077990873379	194.5102289195452	−56.219636231185234	0.8073599700979737
"Ptosis"	"2 – 59[RE]"	""	1.5668705517423225	0.8265566937486285	129.60068385318476	0.000001009717720990011	0.4692190549366513
"Ptosis"	"2 – 34[LE]"	""	1.9192592174949321	0.7591198579720354	429.29265724906776	0.000008969095006250427	0.5306210565985764
"Ptosis"	"2 – 55[RE]"	""	2.204961166571539	0.8515246444572468	107.70009849715221	1.522603071953142 3	0.8104804880505678
"Ptosis"	"2 – 53[RE]"	""	1.6553906409166277	0.3106962918601033	202.9980458592081	$5.713868347356765 \times 10^{-7}$	0.1261026608429714
"Ptosis"	"2 – 46[LE]"	""	2.322047784532598	0.8011178794814411	455.3594609020202	0.8298053336362727	0.7593203913033452
"Ptosis"	"2 – 2[LE]"	""	1.9436779791235468	0.8133690653150573	156.58371162042647	−0.000005572955494 27508	0.4127465149249126
"Ptosis"	"2 – 3[LE]"	""	2.1237675833646876	0.8170291938716648	118.95251630468971	−3.237176741605822	0.4826653611265786
"Ptosis"	"2 – 5[LE]"	""	2.0391375635918845	0.8295507411372246	319.0641780145527	0.07460660035860656	0.5952180819787629
"Ptosis"	"2 – 5[RE]"	""	1.7900617369106564	0.580461267639218	289.0179966532667	0.000161854908924 39702	0.6353287382561554
"Ptosis"	"2 – 30[LE]"	""	1.9603675597306762	0.8811325625671573	112.64301189188059	0.000002341264121241693	0.5217198381202035
"Ptosis"	"2 – 42[LE]"	""	2.4959194789426635	0.6528114739185951	165.2345592700878 3	−34.82226246001048	0.8725882638427246
"Ptosis"	"2 – 65[LE]"	""	1.6147597240221472	0.6281092964431323	175.6189811722908 3	−10.250738588290943	0.4055168009619013
"Ptosis"	"2 – 65[RE]"	""	1.8151823443419983	0.6722278822815031	165.8286610684460 5	0.000002731822547730189	0.6437431739060031
"Ptosis"	"2 – 13[LE]"	""	3.336480551467215	0.656308974017873	234.5095138511998	−2.316693203806551	0.5515784472932435
"Ptosis"	"2 – 13[RE]"	""	3.704656873821303	0.7685942661619549	234.92102274150227	1.128787778848 05	0.6570514395201754
"Ptosis"	"2 – 9[RE]"	""	2.1247386146053713	1.5820076186056273	110.94916767033016	0.29088404025605996	1.025108457915364
"Ptosis"	"2 – 10[LE]"	""	1.304729330200983	0.792933671658109	95.42689007350475	$5.309123309871211 \times 10^{-7}$	0.3309765683449008
"Ptosis"	"2 – 10[RE]"	""	1.5119360813522242	0.6006023027745 73	103.37437483149725	1.4359526184296 1	0.4556877229466043 7
"Ptosis"	"2 – 15[RE]"	""	2.5301480338077873	0.8854940499669689	111.31366996014034	−9.636256523881343	0.6629076619384574
"Ptosis"	"2 – 40[LE]"	""	1.5750285100331192	0.7108719807222778	135.44315476196806	0.2846425728960184 6	0.5985185818777006
"Ptosis"	"2 – 40[RE]"	""	1.6620661079187768	0.7232173394169286	143.03489607116433	−57.421526191 6778	0.9049420971351688
"Ptosis"	"2 – 8[LE]"	""	3.913499120765801	1.3192532884866082	124.63721001135761	−12.302618720828775	0.7840184124069054
"Ptosis"	"2 – 6[LE]"	""	3.52179962948167	1.0930414845110603	180.8797591242045	−21.97800412 38582	1.0768965174356928
"Ptosis"	"2 – 6[RE]"	""	3.07389763410387	0.8973947152331521	134.69561892501528	0.065845977439977 33	0.7743101876501488
"Ptosis"	"2 – 47[LE]"	""	1.1921137061607197	1.0828228759392529	250.6080191880051	$-8.889863352123939 \times 10^{-7}$	0.44786183920349526
"Ptosis"	"2 – 51[RE]"	""	2.5920712608565726	0.7952972483609193	123.1369075608118	−0.000002160988543 64643	0.27916567650817786
"Normal"	"2C17[LE]"	""	2.2712625450551984	0.8914678228726701	109.25352700157964	$3.386380740266759 \times 10^{-7}$	0.5712652325382578
"Normal"	"2C17[RE]"	""	1.6824374486096256	0.8027130334067948	105.35428696184144	$1.135744014391093 \times 10^{-7}$	0.4463675944895713
"Normal"	"2C4[LE]"	""	1.2514522221738984	0.9409348292953218	98.36936702718752	0.000001600596078 78793	0.5059236979462699
"Normal"	"2C4[RE]"	""	0.9218263511075157	0.6374872869383892	117.68730990274341	0.003613204060627595	0.46045883545378585
"Normal"	"2C33[LE]"	""	1.7848746868818957	1.0447670939862925	95.31888197501743	1.884016139614 3458	0.8447551436914686
"Normal"	"2C33[RE]"	""	2.051603054528439	0.994388822812438	111.4191212214113	1.9175271422074331	0.825753855975264
"Normal"	"2C1[LE]"	""	3.1343010583692346	1.10628018633748	114.07220690440796	$2.242230436877435 \times 10^{-7}$	0.48079732295390404
"Normal"	"2C1[RE]"	""	3.038726051390738	1.0087728141437005	116.49353147086683	0.000450977393 6831607	0.4781521248092253
"Normal"	"2C21[LE]"	""	1.6360002589999634	0.5657606460080972	184.81108180660112	6.386909439815952	0.4896164866473619
"Normal"	"2C21[RE]"	""	1.8794576858259526	0.66601756771655	178.28726399991746	3.193829776964293	0.4864431219584003
"Normal"	"2C25[LE]"	""	3.268553063218819	0.9039748201961528	110.48963449432114	1.240194544927192	0.4216979321368702 3
"Normal"	"2C25[RE]"	""	3.419294862698407	0.9642351099140176	103.5104346022311	0.068573308841735 07	0.6484432870200165
"Normal"	"2C19[LE]"	""	1.8359124517606606	1.0852465162344258	184.01108103529145	0.3257035729080826	0.650381320645009
"Normal"	"2C19[RE]"	""	2.5068650811193796	0.8836234043341648	219.49380868781958	−3.724462204764595	0.6179054981784229
"Normal"	"2C23[LE]"	""	3.5835612834380903	1.5588014131211256	126.73346988154208	0.8669675430632253	0.784379061562971
"Normal"	"2C23[RE]"	""	3.0168471121168805	1.1225477735987726	140.80033195984484	−0.053540947896891566	0.48828231972319464
"Normal"	"2C43[LE]"	""	1.4232514200075694	0.8280083872997878	143.80856014170467	−0.000002526393132029625	0.49542529020375864
"Normal"	"2C43[RE]"	""	1.5179491631535635	0.6850703006038039	135.1241043119386	−34.64419371105518	0.6961916866386257
"Normal"	"2C45[LE]"	""	2.6246264280269327	0.9925853631945898	184.50545635995218	−6.058242872200765	0.6956933811002726
"Normal"	"2C45[RE]"	""	2.3692490329535336	0.9512028968491981	187.7912242289271	0.461962259026 5635	0.6082894063258245
"Normal"	"2C6[LE]"	""	1.1443784875401901	0.6386546214833452	145.1639765903745	0.000003569476888287 681	0.3040583101168715
"Normal"	"2C6[RE]"	""	1.4861604268688149	0.7191991505241897	147.05664763312302	$1.412286110280547 \times 10^{-8}$	0.42151522352657134
"Normal"	"2C29[LE]"	""	1.6581600339863554	1.129355339735196	115.26282659880039	0.3075153491987805 4	0.8231379279733134
"Normal"	"2C29[RE]"	""	1.6234806121294196	1.025752558907707	110.0687346933656	1.207281515987716 6	0.7714169633556305
"Normal"	"2C39[LE]"	""	1.6838444131629409	1.2479445985135067	260.898467686466	0.009011981942478542	0.5770618078284132
"Normal"	"2C39[RE]"	""	1.7713120301423588	1.5294147133038416	252.6834670712903	0.000005528078531824576	0.48930537338004276
"Normal"	"2C7[LE]"	""	3.270812588351346	1.2085408449683313	183.4955168367344	$6.063594639726944 \times 10^{-7}$	0.8282234809961908
"Normal"	"2C7[RE]"	""	2.7032336493002185	1.0604799964803695	187.59965803187842	0.041015579849869255	0.641394115469721
"Normal"	"2C11[LE]"	""	1.9305134567547555	1.2372653641224902	86.58930885590499	0.2168073355196043	0.6028121402348943
"Normal"	"2C11[RE]"	""	2.3818977848209073	1.0027877457125696	94.00969072128709	0.7596844923427568	0.8418136597147221
"Normal"	"2C27[LE]"	""	1.6563492237076893	1.08485031543859	104.63730778170722	0.8480509468983541	0.8504927089629816
"Normal"	"2C27[RE]"	""	1.8922389843940755	1.0902010806953213	117.74651122730839	0.8389495925056565	0.7463850140892423
"Normal"	"2C31[LE]"	""	3.0786650042741317	1.0547030366491739	135.03547358195905	−3.0504329112157507	0.8046188834096539
"Normal"	"1C17[LE]"	""	4.199157643944056	1.8110359560234228	81.47100592703413	0.21722924635659524	0.9745259770804 05
"Normal"	"1C17[RE]"	""	4.535630240024286	1.750970556989789	84.69596240614284	0.000001001891845930913	0.8908741617865324
"Normal"	"1C4[LE]"	""	3.124989208773192	1.9554929065141888	88.4641396850271	0.022055371975355342	1.556778260818234
"Normal"	"1C4[RE]"	""	2.505324085981087	2.1209132335006196	88.09628415662 49	1.185908452962039	1.3351422117976646
"Normal"	"1C11[RE]"	""	6.471869053461678	1.9047138638539378	44.656599919700895	$6.131259553399104 \times 10^{-7}$	1.2877284682996095
"Normal"	"1C3[LE]"	""	4.390474095278673	1.6560600291526861	81.490174565643	0.000001073950485874775	0.8413645834774283

Supplementary information 3.| Details of all subjects involved in this part of the test are included here (age ≥40 ptosis vs Controls). The values of minimum, start and end percentages are neglected as they do not have much influence on the shape: v_1, v_2 and α are shown as sharp1, sharp2 and sharp3 on this table, respectively.